Plasmonic nanofocusing with a metallic pyramid and an integrated C-shaped aperture

Nathan C. Lindquist[1,2], Timothy W. Johnson[1], Prashant Nagpal[3], David J. Norris[4] & Sang-Hyun Oh[1,5]

[1]Department of Electrical and Computer Engineering, University of Minnesota, Minneapolis, MN, USA, [2]Physics Department, Bethel University, St Paul, MN, [3]Department of Chemical and Biological Engineering, University of Colorado at Boulder, Boulder, CO, USA, [4]Optical Materials Engineering Laboratory, ETH Zürich, Zürich, Switzerland, [5]Department of Biophysics and Chemical Biology, Seoul National University, Seoul, Korea.

We demonstrate the design, fabrication and characterization of a near-field plasmonic nanofocusing probe with a hybrid tip-plus-aperture design. By combining template stripping with focused ion beam lithography, a variety of aperture-based near-field probes can be fabricated with high optical performance. In particular, the combination of large transmission through a C-shaped aperture aligned to the sharp apex (<10 nm radius) of a template-stripped metallic pyramid allows the efficient delivery of light—via the C-shaped aperture—while providing a nanometric hotspot determined by the sharpness of the tip itself.

Metallic nanostructures that support surface plasmons[1,2]— an electromagnetic wave that is confined to the metallic interface — allow deep sub-wavelength control of light. This near-field manipulation of light offers many unique applications in the emerging field of plasmonics[3–9]. In particular, plasmonic nano-focusing has shown great promise by enabling, for example, nanoscale light sources, tip-enhanced Raman spectroscopy, and unprecedented optical imaging resolution[10–15]. All nanoscale metallic tips exhibit local electric field enhancements due to an electrostatic lightning rod effect. However, stronger field enhancements and tighter confinements can be achieved by launching surface plasmons towards a tip, which enables an efficient delivery of optical energy into a nanoscale volume at the apex[10,12,14,16,17]. As the lateral dimensions of the metallic structure become smaller, the propagating surface plasmon is effectively squeezed into the localized surface plasmon at the tip. The final spatial extent of the surface plasmon can be effectively determined by the sharpness of the tip itself and is associated with large field enhancements.

When a surface plasmon waveguide is tapered adiabatically[12], i.e. slowly compared to the plasmon wavelength, reflections are minimized and the plasmon freely propagates towards the tip. However, as the field becomes more localized within the metal, dissipation increases substantially. Furthermore, if the taper angle is on the order of a few degrees, the taper length will be quite long, also increasing dissipation. Conversely, non-adiabatic schemes use a relatively large taper angle in an effort to minimize propagative losses. Unfortunately, significant reflections may result, decreasing the delivery of energy to the tip. With these two competing effects, it may be possible to design a structure with an optimal taper angle[18]. In either case, plasmonic nanofocusing at the apex of a sharp metallic tip requires precise control and design of the delivery scheme. If possible, it is beneficial to allow the optical energy to propagate in a low-loss dielectric medium until diffractive effects dominate. Waiting until that point before conversion to a surface plasmon waveguide and nanofocusing tip structure will minimize overall losses. Most metallic tips and tapers are fabricated with metal deposition, the metallization of fibers, or with electrochemical etching[19–21]. Electron-beam induced deposition has also been used[22,23]. Often, the devices are then patterned with focused ion beam (FIB) milling. Unfortunately, the surface roughness of as-deposited metals can be detrimental to any desired nanofocusing effect. This motivates the use of a template-stripping method to produce smoothly patterned interfaces and sharp tips[20,24,25].

Previously, to launch surface plasmons towards a sharp gold tip, gratings have been milled into the side of an electrochemically etched gold wire[13]. Likewise, the use of nanohole gratings next to a region with a laterally tapered thin gold film have also been demonstrated[14]. In a different scheme, curved slits[26–28] or holes[29] focus plasmons to an in-plane bright spot. Full three-dimensional nanofocusing is also possible, with, for example, radially polarized plasmons propagating along a circularly symmetric tapered waveguide[30]. The use of radial polarization is necessary since as the plasmons travel towards the tip, the fields on opposing sides of the waveguide

should interfere constructively. This results in a longitudinal electric field at the tip, i.e. along the tip axis. Illumination with linearly polarized light at normal incidence does not have the necessary field symmetry, and requires illumination at a large tilt angle[31], or the use of an asymmetric tip[11]. Alternatively, the edges of tightly focused Gaussian beams are able to excite the longitudinal mode of the tip[32]. Previously, we demonstrated a three-dimensional plasmonic nanofocusing pyramid with asymmetric patterning that can be excited with normally incident linearly polarized light[25]. With unpatterned pyramids and radially polarized light, we have also shown that template-stripped pyramids incorporated into a near-field scanning optical microscope (NSOM) give large (>200×) enhancements in the detected single-molecule fluorescence signal with <20 nm spatial imaging resolution[33]. However, backside or internal illumination schemes are also beneficial, opening up a wider variety of sample probing geometries and the use of opaque samples. Since the illumination is internal to the tip, background light is minimized. While aperture NSOM tips are well established[34], the ultimate spatial resolution is determined by the size of the aperture. Unfortunately, small (<100 nm) apertures have limited optical throughput and the skin depth of real metals effectively increases the size of the aperture. While throughput can be increased by exploiting enhanced transmission effects[35], the spatial resolution is still limited. To improve the spatial resolution while keeping the low-background noise, a tip-on-aperture design has been used whereby a small opening illuminates a protruding metallic tip[36]. Other hybrid designs such as coaxial tips[37] or metal-insulator-metal (MIM) waveguides[38] have also been considered.

In this paper, we show a new device fabricated via template stripping and precision FIB milling for backside, high-intensity plasmonic nanofocusing. We combine the smooth interfaces and sharp tips produced via template stripping with the efficient delivery of optical energy via a high-transmission C-shaped aperture. It is known that changing the shape of a subwavelength aperture can dramatically change its transmission properties[39,40]. Our design integrates a tip-on-aperture device[36,41], with a high-transmission C-shaped aperture[42,43]. The asymmetry of the C-shape allows internal illumination with normal-incidence, linearly polarized light, with efficient delivery of the optical energy to a sharp (<10 nm radius) template-stripped pyramidal tip.

Results

To fabricate our silver pyramids, we used template-stripping techniques[24,44] that take advantage of the poor adhesion of silver to silicon. When silver is deposited onto a silicon wafer, it is easily peeled off and removed with an adhesive backing layer. Using established micro-fabrication techniques, the silicon wafer is easily patterned, producing a negative replica template for the silver film. With anisotropic etching of silicon with potassium hydroxide (KOH), template stripping can thus produce sharp metallic tips[24] suitable for plasmonic nanofocusing[25] and near-field imaging[33]. Likewise, template stripping can produce apertures either as part of the template[24,45,46] or with backside FIB milling, as shown here. To fabricate our structures, we first created a silicon template (figure 1a) and then deposited a 200 nm-thick layer of silver (figure 1b). FIB milling then defined openings through the silver film (figure 1c). On this side of the film, FIB exposure and any implanted ions or induced roughness is not critical, and FIB milling through the backside of a metallic film has been shown to reduce unwanted edge rounding of the aperture[47]. Finally, the silver film was glued to a glass microscope slide (figure 1d) and removed from the template (figure 1e). The final pyramid is hollow—i.e. filled with transparent optical-grade epoxy—and retains a sharp tip, untouched by the FIB (figure 1f), and the smooth template-stripped surface.

Figure 2 shows scanning electron micrographs (SEMs) of the fabricated devices. The C-shaped aperture is situated around the sharp
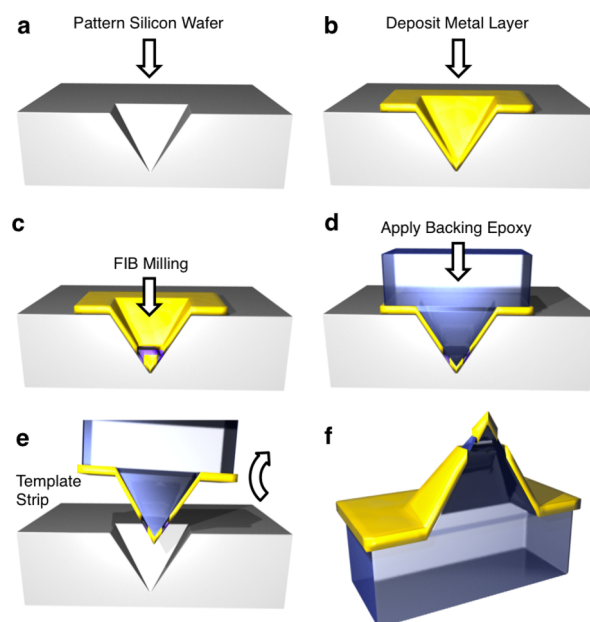

Figure 1 | Processing schematic. (a) A silicon template is patterned with anisotropic KOH etching with an SiO_2 etch mask. (b) A thin metal layer is deposited. (c) FIB milling is used to define the tip aperture shape. (d) An optical epoxy layer is applied. (e) The pyramid with an integrated aperture is stripped from the template on demand. (f) The final hollow tip retains an ultrasharp tip untouched by the FIB.

tip of the silver pyramid. Angled SEMs in figure 2b and 2d show the three-dimensional nature of the device. The three legs of the C-shaped aperture have a width of 100 nm and cover a 400-by-400 nm area. Multiple devices can be fabricated (figure 2c) and each tip can be stored in the silicon template for extended periods (>1 year) and used "on-demand" for NSOM imaging[33]. Standard circular aperture structures (diameter 125 nm) can also be fabricated with this method, shown in figures 2e and 2f. With this hybrid C-shaped aperture plus sharp pyramidal tip design, the sharp metallic tip is positioned away from the C-shaped slits, allowing the dual benefits of both high transmission just below the tip and tight field confinement at the tip. Furthermore, the relatively large taper angle of our pyramids (70.5°) — determined by the crystalline facets of the silicon template — allows easy optical access to the tip and aperture region from the backside. A long and narrow tapered structure, for example, could not be illuminated internally since light would not propagate all the way to the aperture due to waveguide cut-off[19], and a solid wire would require precise butt-end coupling[48]. Previously, planar C-apertures have been shown to offer large resonant transmission effects[43], and have been suggested as an efficient near-field probe candidate[49]. Our structures, while resembling the C-aperture design, have a distinct three-dimensional shape where the metallic "tongue" of the C is lifted vertically and incorporated into the sharp tip of the square pyramids, as with a tip-on aperture device. The tip itself is not fabricated via FIB or exposed to any processing. This keeps the tip sharp (<10 nm radius) and free from roughness and contamination. As will be discussed below, it is the asymmetric arrangement of the three segments of the C around the tip that allows the efficient generation of surface plasmons that propagate and focus at the tip.

Discussion

To reveal the expected behavior of the C-shaped slits, full three-dimensional finite-difference time-domain (FDTD) simulations were performed. The pyramid tip points in the +z axis, and the tongue of the C-shaped aperture is aligned along the x-axis. These results are shown in figure 3. Two scenarios were simulated: a full
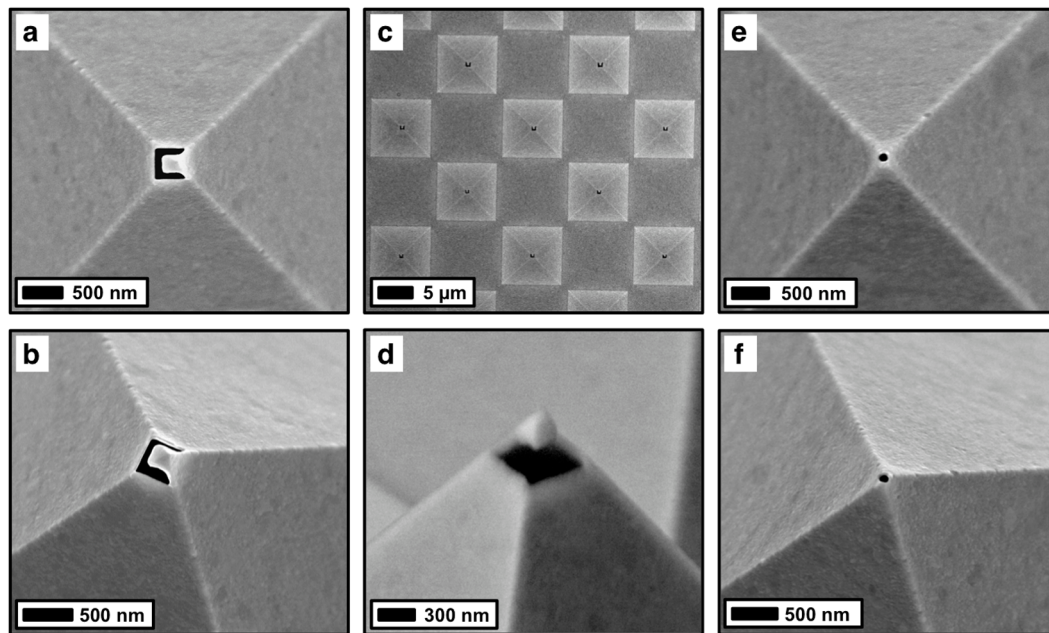
Figure 2 | Scanning electron micrographs (SEMs) of the pyramid and aperture structures. (a) Top-down SEM of a C-shaped aperture placed right at the apex. (b) Angled view of the same pyramid. (c) Multiple pyramids can be fabricated by aligned FIB milling. (d) Side-view SEM of the structure, showing the metallic tip above the aperture. (e) With this method, circular apertures are also possible. (f) Angled view of a ~130 nm diameter circular aperture.
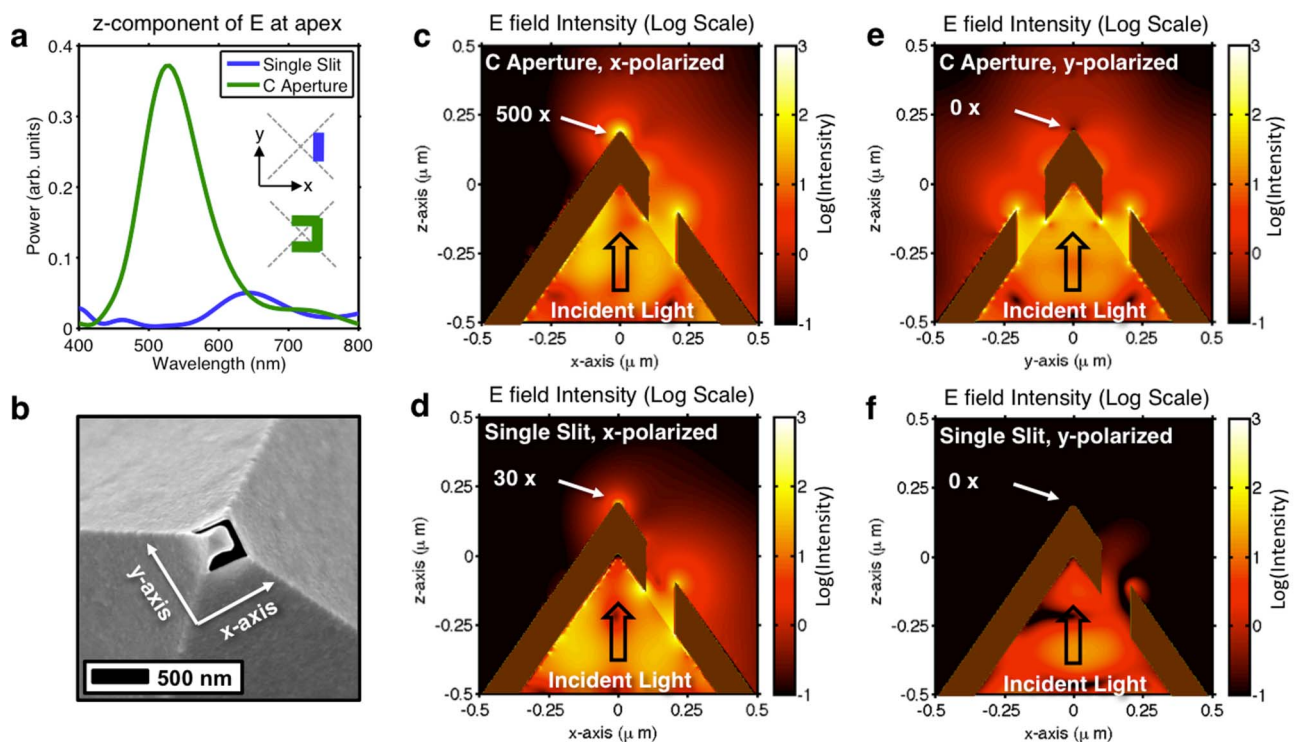

Figure 3 | Finite-difference time-domain (FDTD) simulations of the C-shaped aperture. (a) Spectral response of the z-component of the electric field at the tip showing a large resonant peak at 530 nm. Transmission through a single slit—the C-shaped aperture has three slits—is shown to be much weaker. The light was x-polarized (horizontally with respect to the inset schematics as shown on the axes). (b) SEM of a C-aperture device illustrating the coordinate axes used. (c) Steady-state maps of the electric field intensity of a C-shaped aperture device at the resonant wavelength. Illuminating from below with x-polarized light generates plasmons at the apex. The color scale represents the log of the field intensity enhancement. (d) For a device comprising only a single slit, the field intensity enhancement at the apex is much less. (e) For y-polarized light, the fields from opposite arms of the C-shaped aperture interfere destructively at the tip. Note that in this panel, the cross-section is along the y-axis. (f) For y-polarized light illuminating a single slit, there is negligible transmission through the slit and plasmons are not generated.

C-shaped aperture and a single-slit aperture on one face of the pyramid. These two designs are shown in the inset of figure 3a, as are the coordinate axes used (also shown for reference in figure 3b). The spectral behaviors are shown in the plot of figure 3a, where the z-component of the electric field directly above the apex of the pyramid was Fourier-transformed from a time-pulsed input beam. The incident light was x-polarized. As is seen, the single slit aperture does transmit and generate surface plasmons that converge at the tip. However, the field intensity is low. The C-shaped slit arrangement, however, displays a large peak at 530 nm, signifying the resonant behavior of the device. Steady-state x-z cross-sectional field maps at 530 nm illumination are shown in figure 3c. The electric field intensity enhancement at the tip, normalized to the intensity just below the aperture inside the pyramid, is >500×. In contrast, the field intensity enhancement of the single-slit aperture (figure 3d) is only ~30×. While surface plasmons are generated and launched from the single slit, clearly the unique geometry of the C-shaped slit arrangement is critical for high transmission[43]. Additionally, the asymmetry of the C-shaped slit aperture is critical for achieving plasmonic nanofocusing with normally incident, linearly polarized light. Indeed, large field intensity enhancements at the tip are only seen when the incident light is x-polarized along the tongue of the C-shaped slit aperture. Figure 3e shows a cross-sectional field map of the pyramid with y-polarized illumination. In this case, there is an intensity null at the tip, since surface plasmons launched from both sides — i.e. from each "arm" of the C — arrive out-of-phase, producing destructive interference at the apex[25]. Finally, changing the polarization for a single slit aperture also results in negligible intensity at the tip (figure 3f).

The optical behavior of slits—similar to figure 3d—located on the face of a pyramid is studied in figure 4. Here, an array of slits was situated 4.5 μm from the tip of the pyramid (measured along the face). Figure 4a shows an SEM of the device before template stripping but after patterning the slits via FIB milling. Figure 4b shows the device after template stripping. With laser illumination from below (633 nm), light is seen to transmit through the slits but also to scatter from the tip region. By changing the polarization (figure 4d), the transmission through the slits is minimized, and no light is seen at the tip. These experiments suggest that plasmons are indeed excited by the slits and travel upwards towards the apex of the pyramid, as demonstrated computationally in figure 3d.

For experimental characterization of the fabricated aperture devices, the transmission spectra of two flat aperture designs are shown in figure 5. Figure 5a shows a single nanohole milled through a flat 200 nm thick silver film as well as a C-shaped aperture milled on the same substrate. These apertures were fabricated with backside FIB milling and template stripping as before. Figure 5b shows the large transmission of the C-shaped aperture as compared to the single nanohole. The low transmission of a single nanohole aperture placed on a pyramidal tip—a standard NSOM probe and shown in figures 2e,f—is a significant drawback. By instead using a C-shaped aperture, more transmission is seen. The transmission is also shown to be dependent on the incident polarization.

Figure 6 demonstrates the far-field optical transmission through C-shaped apertures placed on pyramids. Figure 6a shows a microscope image with illumination from the top and bottom (internal) sides of both a nanohole aperture and a C-shaped aperture. The transmission through the C-shaped aperture is significantly brighter than the transmission from the single-hole apertures. Figure 6b
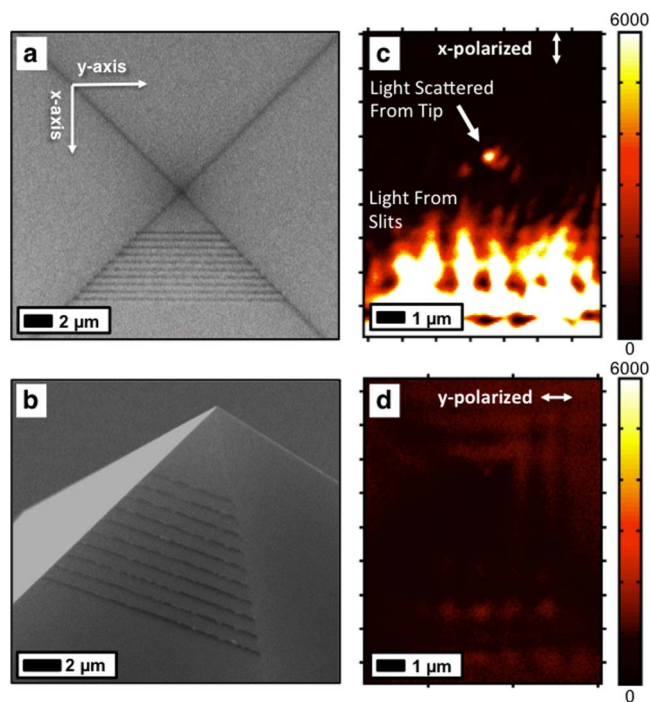

Figure 4 | Pyramid with slit apertures. (a) SEM of a 200 nm thick silver pyramid sample before template stripping but after FIB milling. The axes shown are consistent with the FDTD models of figure 3. (b) SEM after template stripping. (c) The slits are used to launch surface plasmons up the face of the pyramid where they scatter from the tip and are collected by the microscope. Note that the microscope image is in the same orientation as the SEM image in panel (a). (d) By changing the incident polarization (to y-polarized), plasmons are no longer generated in the device.
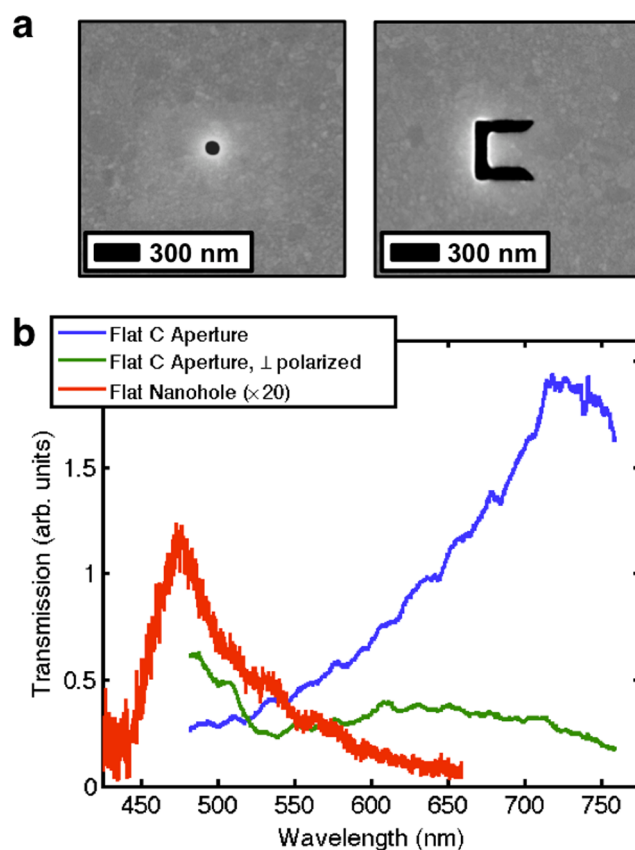

Figure 5 | Optical transmission measurements of apertures through a flat template-stripped Ag film. (a) SEM of a single nanohole and of a C-shaped aperture. (b) The single nanohole weakly transmits blue light, while the C-shaped aperture strongly transmits red light with a polarization dependence. Light polarized along the tongue of the C (in the *x*-direction) transmits most efficiently.
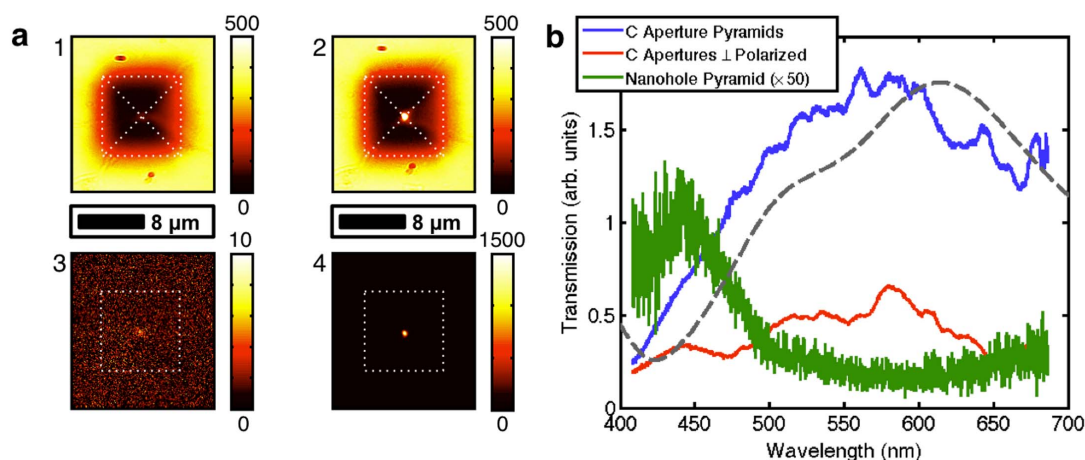
Figure 6 | Optical transmission measurements through pyramid apertures. (a) Bright-field image of (1) a nanohole pyramid and (2) a C-shaped aperture pyramid with internal white light illumination. The dashes represent the base of the pyramids. Eliminating the bright-field illumination shows transmission only through (3) the nanohole and (4) the C-shaped apertures themselves. With these images, the peak intensity of the C-shaped aperture appears 150× brighter. (b) Examining the spectral transmission of the C-shaped aperture shows a broad peak, largely consistent with FDTD (dashed gray line) results. The transmission also depends on the polarization. Compared to a pyramid with a single nanohole (figure 2e, f), the peak transmission is shifted to the red and more than 50× more intense.

shows an experimental far-field transmission spectrum (averaged from several devices) along with FDTD calculations. The shift in the FDTD peak position compared to experiment could be from the exact manner in which the epoxy fills the apertures or from the rounding of the aperture edges from the FIB. The broad transmission peak near 600 nm shows the large far-field transmission. The flat aperture spectra of figure 5 can also help identify how the three-dimensional nature of the pyramid tip affects an aperture's properties. The nanohole aperture has similar spectral behavior (peak at ~450 nm) on both a flat substrate and at the apex of the pyramid. The C-shaped aperture, however, has a distinct shift (~700 nm flat to ~600 nm on the pyramid). We believe shift this is due to the three-dimensional shape (figure 2) that the C-shaped aperture acquires when placed at the apex of the pyramid. Finally, it should be noted that the near-field behavior is inaccessible in these experiments but has been elucidated via FDTD in figure 3.

In conclusion, we have demonstrated a unique design for a high-intensity near-field aperture probe based on the placement of a C-shaped aperture around the tip of a sharp (10 nm) template-stripped pyramid. The tip offers polarization-dependent control and illumination with linearly polarized, normally incident light. This makes our tip more forgiving to misalignment compared to illumination with a radially polarized beam since the light is effectively "channeled" by the underside of the converging pyramid towards the aperture. As shown by our FDTD simulation results, these tips display large field intensity enhancements and could offer several advantages where high optical throughput, high resolution, and low background noise are needed, such as in NSOM and tip-enhanced Raman spectroscopy.

Methods

To fabricate our structures, we first created a silicon template with anisotropic KOH etching. Standard optical lithography was used to pattern 8 μm square openings in a 100 nm thick thermally grown SiO_2 layer. The wafer was then etched in 20% KOH at 60°C for 90 minutes and the oxide was removed via wet etching in buffered oxide etchant for. Next, a 200 nm-thick layer of silver was deposited via e-beam deposition at an initial rate of 0.1 Å/s ramping to a rate of 1 Å/s at the end. After this, FIB milling (30 kV, 10 pA) defined the openings through the silver film. The backsides of the pyramids were briefly imaged with the FIB and the beam shifted to obtain precise alignment. Finally, the silver film was glued (Norland Products, NOA61) to a standard glass microscope slide and stripped from the silicon template.

Computer simulations used a commercial FDTD package (FullWAVE, RSoft Design Group). The dielectric function of the silver was fit with a Drude/Lorentz model to experimental ellipsometry data of a flat template stripped film.

A non-uniform grid was used that was 6 nm in the bulk and tapered to 2 nm at the tip in the x and y directions and 1 nm in the z direction. The tip had a radius of 10 nm and the refractive index of the epoxy was taken to be 1.56. Perfectly matched layers were used to prevent reflections from the 1.6 μm × 1.6 μm × 2 μm simulation volume boundaries. A pulsed x-polarized wave was incident from the bottom-side of the pyramid. The z-component of the electric field was then Gaussian transformed to determine the spectral response of the tip. Steady-state field maps were then created with continuous wave illumination at the desired wavelength.

Experimental optical transmission spectra and images were recorded with an inverted microscope (Nikon Eclipse, 100× objective, NA = 0.9) coupled to an imaging spectrometer (Newport MS 257) with a deep-cooled CCD camera (Princeton Instruments, Pixis). The light was linearly polarized and the transmission spectra of the different devices were normalized to the spectrum of the illumination lamp.

1. Ritchie, R. Plasma losses by fast electrons in thin films. *Phys. Rev.* **106**, 874 (1957).
2. Raether, H. *Surface Plasmons on Smooth and Rough Surfaces and on Gratings.* 1–140 (Springer-Verlag, 1986).
3. Barnes, W. L., Dereux, A. & Ebbesen, T. W. Surface plasmon subwavelength optics. *Nature* **424**, 824–830 (2003).
4. Maier, S. A. *et al.* Local detection of electromagnetic energy transport below the diffraction limit in metal nanoparticle plasmon waveguides. *Nature Materials* **2**, 229–232 (2003).
5. Lal, S., Link, S. & Halas, N. J. Nano-optics from sensing to waveguiding. *Nature Photonics* **1**, 641–648 (2007).
6. Homola, J. Surface Plasmon Resonance Sensors for Detection of Chemical and Biological Species. *Chem. Rev.* **108**, 462–493 (2008).
7. Bharadwaj, P., Deutsch, B. & Novotny, L. Optical antennas. *Adv. Opt. Photon.* **1**, 438–483 (2009).
8. Atwater, H. A. & Polman, A. Plasmonics for improved photovoltaic devices. *Nature Materials* **9**, 205–213 (2010).
9. Novotny, L. & van Hulst, N. F. Antennas for light. *Nature Photonics* **5**, 83–90 (2011).
10. Babadjanyan, A., Margaryan, N. & Nerkararyan, K. V. Superfocusing of surface polaritons in the conical structure. *J. Appl. Phys.* **87**, 3785–3788 (2000).
11. Sanchez, E., Novotny, L. & Xie, X. Near-field fluorescence microscopy based on two-photon excitation with metal tips. *Phys. Rev. Lett.* **82**, 4014–4017 (1999).
12. Stockman, M. I. Nanofocusing of optical energy in tapered plasmonic waveguides. *Phys. Rev. Lett.* **93**, 137404 (2004).
13. Ropers, C. *et al.* Grating-Coupling of Surface Plasmons onto Metallic Tips: A Nanoconfined Light Source. *Nano Lett.* **7**, 2784–2788 (2007).
14. Verhagen, E., Polman, A. & Kuipers, L. K. Nanofocusing in laterally tapered plasmonic waveguides. *Opt. Express* **16**, 45–57 (2008).
15. De Angelis, F. *et al.* Nanoscale chemical mapping using three-dimensional adiabatic compression of surface plasmon polaritons. *Nature Nanotech.* **5**, 67–72 (2010).
16. Novotny, L., Bian, R. & Xie, X. Theory of nanometric optical tweezers. *Phys. Rev. Lett.* **79**, 645–648 (1997).
17. Berweger, S., Atkin, J. M., Olmon, R. L. & Raschke, M. B. Light on the Tip of a Needle: Plasmonic Nanofocusing for Spectroscopy on the Nanoscale. *J. Phys. Chem. Lett.* **3**, 945–952 (2012).

18. Issa, N. A. & Guckenberger, R. Optical Nanofocusing on Tapered Metallic Waveguides. *Plasmonics* **2**, 31–37 (2007).

19. Novotny, L. & Hecht, B. *Principles of Nano-Optics.* (Cambridge Univ Press, 2012).

20. Lindquist, N. C., Nagpal, P., McPeak, K. M., Norris, D. J. & Oh, S.-H. Engineering metallic nanostructures for plasmonics and nanophotonics. *Rep. Prog. Phys.* **75**, 036501 (2012).

21. Fleischer, M. Near-field scanning optical microscopy nanoprobes. *Nanotechnol. Rev.* **1**, 313–338 (2012).

22. De Angelis, F. *et al.* Breaking the diffusion limit with super-hydrophobic delivery of molecules to plasmonic nanofocusing SERS structures. *Nature Photonics* **5**, 682–687 (2011).

23. Acar, H., Coenen, T., Polman, A. & Kuipers, L. K. Dispersive Ground Plane Core–Shell Type Optical Monopole Antennas Fabricated with Electron Beam Induced Deposition. *ACS Nano* **6**, 8226–8232 (2012).

24. Nagpal, P., Lindquist, N. C., Oh, S.-H. & Norris, D. J. Ultrasmooth Patterned Metals for Plasmonics and Metamaterials. *Science* **325**, 594–597 (2009).

25. Lindquist, N. C., Nagpal, P., Lesuffleur, A., Norris, D. J. & Oh, S.-H. Three-Dimensional Plasmonic Nanofocusing. *Nano Lett.* **10**, 1369–1373 (2010).

26. López-Tejeira, F. *et al.* Efficient unidirectional nanoslit couplers for surface plasmons. *Nature Phys.* **3**, 324–328 (2007).

27. Chen, W., Abeysinghe, D. C., Nelson, R. L. & Zhan, Q. Plasmonic Lens Made of Multiple Concentric Metallic Rings under Radially Polarized Illumination. *Nano Lett.* **9**, 4320–4325 (2009).

28. Kim, H. *et al.* Synthesis and Dynamic Switching of Surface Plasmon Vortices with Plasmonic Vortex Lens. *Nano Lett.* **10**, 529–536 (2010).

29. Yin, L. *et al.* Subwavelength Focusing and Guiding of Surface Plasmons. *Nano Lett.* **5**, 1399–1402 (2005).

30. Bouhelier, A., Renger, J., Beversluis, M. & Novotny, L. Plasmon-coupled tip-enhanced near-field optical microscopy. *J. Microsc.* **210**, 220–224 (2003).

31. Roth, R. M. *et al.* Resonant-plasmon field enhancement from asymmetrically illuminated conical metallic-probe tips. *Opt. Express* **14**, 2921 (2006).

32. Bouhelier, A., Beversluis, M., Hartschuh, A. & Novotny, L. Near-Field Second-Harmonic Generation Induced by Local Field Enhancement. *Phys. Rev. Lett.* **90**, 013903 (2003).

33. Johnson, T. W. *et al.* Highly Reproducible Near-Field Optical Imaging with Sub-20-nm Resolution Based on Template-Stripped Gold Pyramids. *ACS Nano* **6**, 9168–9174 (2012).

34. Betzig, E. & Trautman, J. K. Near-field optics: microscopy, spectroscopy, and surface modification beyond the diffraction limit. *Science* **257**, 189 (1992).

35. Neumann, L. *et al.* Extraordinary Optical Transmission Brightens Near-Field Fiber Probe. *Nano Lett.* **11**, 355–360 (2011).

36. Frey, H. G., Keilmann, F., Kriele, A. & Guckenberger, R. Enhancing the resolution of scanning near-field optical microscopy by a metal tip grown on an aperture probe. *Appl. Phys. Lett.* **81**, 5030–5032 (2002).

37. Weber-Bargioni, A. *et al.* Hyperspectral nanoscale imaging on dielectric substrates with coaxial optical antenna scan probes. *Nano Lett.* **11**, 1201–1207 (2011).

38. Choo, H. *et al.* Nanofocusing in a metal–insulator–metal gap plasmon waveguide with a three-dimensional linear taper. *Nature Photonics* **6**, 838–844 (2012).

39. Gordon, R. *et al.* Strong Polarization in the Optical Transmission through Elliptical Nanohole Arrays. *Phys. Rev. Lett.* **92** (2004).

40. van der Molen, K. L., Segerink, F. B., van Hulst, N. F. & Kuipers, L. Influence of hole size on the extraordinary transmission through subwavelength hole arrays. *Appl. Phys. Lett.* **85**, 4316–4318 (2004).

41. Taminiau, T., Stefani, F., Segerink, F. & van Hulst, N. F. Optical antennas direct single-molecule emission. *Nature Photonics* **2**, 234–237 (2008).

42. Shi, X., Hesselink, L. & Thornton, R. Ultrahigh light transmission through a C-shaped nanoaperture. *Opt. Lett.* **28**, 1320–1322 (2003).

43. Lee, B., Lee, I. M., Kim, S., Oh, D. H. & Hesselink, L. Review on subwavelength confinement of light with plasmonics. *J. Mod. Optic.* **57**, 1479–1497 (2010).

44. Hegner, M., Wagner, P. & Semenza, G. Ultralarge Atomically Flat Template-Stripped Au Surfaces for Scanning Probe Microscopy. *Surf. Sci.* **291**, 39–46 (1993).

45. Im, H. *et al.* Template-Stripped Smooth Ag Nanohole Arrays with Silica Shells for Surface Plasmon Resonance Biosensing. *ACS Nano* **5**, 6244–6253 (2011).

46. Lindquist, N. C., Johnson, T. W., Norris, D. J. & Oh, S.-H. Monolithic Integration of Continuously Tunable Plasmonic Nanostructures. *Nano Lett.* **11**, 3526–3530 (2011).

47. Leen, J. B., Hansen, P., Cheng, Y.-T. & Hesselink, L. Improved focused ion beam fabrication of near-field apertures using a silicon nitride membrane. *Opt. Lett.* **33**, 2827–2829 (2008).

48. Chen, X.-W., Sandoghdar, V. & Agio, M. Highly Efficient Interfacing of Guided Plasmons and Photons in Nanowires. *Nano Lett.* **9**, 3756–3761 (2009).

49. Cheng, Y. T. *et al.* Ultra-high resolution resonant C-shaped aperture nano-tip. *Opt. Express* **19**, 5077–5085 (2011).

Acknowledgements

Author contributions

N.C.L. and T.W.J. fabricated the samples, took SEM images, and performed the optical experiments. P.N. fabricated samples and took SEM images. N.C.L. performed the FDTD computer simulations. N.C.L., S.H.O. and D.J.N. conceived the structure and the experiments. All authors contributed in writing the manuscript.

Additional information